Efficient Denoising of Multidimensional GPR Data Based on Fast Dictionary Learning

Deshan Feng, Li He, Xun Wang, Yougan Xiao, Guoxing Huang, Liqiong Cai, and Xiaoyong Tai

***Abstract*—Denoising plays a fundamental role in ground penetrating radar (GPR) data processing and determines the effect of anomaly extraction, inversion imaging, and other subsequent processing. In recent years, the sparse dictionary representation method k-singular value decomposition (K-SVD) based on K-means, which can adaptively change the basis function according to the data, has become a hotspot in the field of image denoising and data reconstruction. Nevertheless, the SVD is a time-consuming calculation, especially unacceptable in multidimensional problems; we introduce a dictionary learning method based on the sequential generalized K-means (SGK), where the dictionary atoms are updated by the arithmetic average of several training signals instead of a great deal of SVD calculation in K-SVD. We establish a 3-D road simulation model and conduct finite-difference time-domain forward numerical simulation to acquire 3-D GPR data. Through three sets of experiments on 3-D numerical examples and 3-D field data, the results show that both dictionary learning algorithms can successfully remove random noise from GPR data even at a lower input signal-to-noise ratio. The clutter interference in the random medium forward data can be effectively eliminated simultaneously, and both denoising methods exhibit promising applications in 3-D field data. However, the SGK method solves the serious problem of computational efficiency to a certain extent. The computational acceleration ratio of SGK remains consistently above 7.5× that of the K-SVD algorithm in multigroup experiments, with only a marginal decline in denoising performance.**

***Index Terms*—Dictionary learning, ground penetrating radar (GPR), K-singular value decomposition (K-SVD), noise attenuation, sparse representation, sequential generalized K-means (SGK).**

I. Introduction

Ground penetrating radar (GPR), as an efficient nondestructive exploration method, can quickly and intuitively obtain the distribution of underground targets in actual exploration. It has the advantages of high precision and high resolution and is often used in environmental, geological applications [1], [2], [3] and engineering exploration [4], [5], [6], among other fields. However, in field acquisition, due to the complex distribution of underground media, environmental interference, and other factors, the GPR data often contain strong background clutter and various random noises [7], [8]. Therefore, to overcome the nonuniform and nonstationary characteristics of the signals, effectively suppress the noises in the GPR echo signals, and highlight the reflected wave, scholars have proposed many denoising methods, which can be roughly divided into four groups: those based on spatial filtering, transform domain, subspace, and deep learning.

The spatial filtering method suppresses the random interference mainly from the point of the difference of spectrum signature. Xiao and Liu [9] developed a multibandpass filtering, which appears superior in the suppression of clutter interference generated by periodic scatterers in GPR data. Kumlu and Erer [10] presented a novel clutter removal method based on nonlocal means, which can efficiently reconstruct GPR images but is limited to low-level noise. Aiming at the nonstationarity of GPR signals, He et al. [11] proposed a self-guided filter combined with edge information for the denoising process in real time. Fourier transform and wavelet transform are first applied to random clutter suppression and direct wave elimination of GPR data by Starck et al. [12] but the memory consumption of this algorithm is unsatisfactory [13]. To optimize the performance of wavelet denoising, discrete wavelet transforms [14] and dual-tree complex wavelet transform [15] have been applied to GPR data denoising. In the multidimensional case, in order to compensate for the finiteness of the direction of the wavelet transforms time base, the multiscale geometric analysis method is introduced, such as the typical Ridgelet transform [16], Shearlet transform [17], [18], and Curvelet transform [19], [20].

Image denoising methods based on subspace mainly include principal component analysis (PCA), singular value decomposition (SVD), and independent component analysis. These methods can be regarded as a dimension reduction algorithm. Chen et al. [21] realized the adaptive clutter reduction of GPR data by the PCA of ground clutter. Su et al. [22] proposed a novel clutter suppression method based on principal component Gaussian curvature decomposition. The complete ensemble empirical mode decomposition (CEEMD) is used in GPR signal processing with a higher spectral–spatial resolution [23]. There, the combination of the improved CEEMD and the multiscale PCA overcomes the limitations of manual mode selection [24]. A method based on the SVD of a

Manuscript received 25 November 2023; revised 20 January 2024; accepted 9 February 2024. Date of publication 15 February 2024; date of current version 28 February 2024. This work was supported in part by the National Natural Science Foundation of China under Grant 42104143 and Grant 42074161 and in part by the Natural Science Foundation of Hunan Province under Grant 2022JJ40584 and Grant 2021JJ30806. *(Corresponding author: Xun Wang.)*

Deshan Feng is with the School of Geosciences and Info-Physics, Central South University, Changsha 410083, China, and also with the School of Earth Sciences, East China University of Technology, Nanchang 330013, China (e-mail: fengdeshan@126.com).

Li He and Xun Wang are with the School of Geosciences and Info-Physics, Central South University, Changsha 410083, China (e-mail: he_li@csu.edu.cn; wangxun@csu.edu.cn).

Yougan Xiao, Guoxing Huang, Liqiong Cai, and Xiaoyong Tai are with the Fuzhou City Construction Design and Research Institute, Fuzhou 350001, China.

Digital Object Identifier 10.1109/JSTARS.2024.3366397

window-length-optimized Hankel matrix [25] is applied to denoise the GPR raw data, and the denoising performance is improved, compared with the traditional SVD method and wavelet transform. Oliveira et al. [26] proposed a method to filter the clutter reflection noise based on SVD for GPR data but the level of automation is insufficient. Although these traditional GPR image-denoising methods can suppress noise to a certain extent, there are always some shortcomings. In the conventional GPR data denoising processing, a set of fixed transformation bases is mainly used, but there is still signal-noise aliasing after denoising.

Soon afterward, dictionary learning methods that can adaptively change the basis function according to the characteristics of data have been proposed and have a great achievement in image denoising and reconstruction, medical imaging, and some other fields [27], [28], [29]. The basic signals have enough sparse representation on the dictionary, while the random noise does not, the dictionary learning method can separate the noise from the effective signals and achieve the purpose of denoising [30], [31]. Constructing an applicable dictionary is an obbligato part of sparse representation, it will affect the speed of sparse computing and exist as the key that determines the quality of sparse representation. The dictionary can be divided into fixed dictionary and adaptive learning dictionary, such as commonly used wavelet dictionary, discrete cosine transform (DCT) dictionary, curvelet dictionary, and so on. Aharon et al. [32] proposed the K-Singular value decomposition (K-SVD) dictionary based on K-means clustering, which is the most representative and widely used in adaptive learning dictionary algorithms. Shortly, Elad and Aharon [33] realized image denoising through the K-SVD dictionary and sparse representation.

Recently, with the development of artificial intelligence, deep learning has been widely used in geophysical data processing [34], [35] and interpretation. Luo et al. [36] proposed a multiscale convolutional autoencoder (MCAE) to fix the denoising task of GPR data and used the data augmentation strategy named Wasserstein generative adversarial network to increase the training dataset of MCAE. A new data-driven method based on conditional generative adversarial networks is used for clutter suppression of GPR data by Ni et al. [37]. Sun et al. [38] introduced the clutter removal neural network, which is trained with large-scale mixed datasets. These networks have excellent ability in data denoising but the research is limited to 2-D datasets.

With the upgrading of hardware facilities, the demand for 3-D GPR technology has been gradually promoted, especially in the fields of archaeological and heritage protection [39], [40], [41] and urban road detection [42], [43], [44]. Efficient 3-D GPR data acquisition brings massive data information, with the multichannel data acquisition method of 3-D GPR bringing more abundant and complex noise sources. At present, there are few studies on the denoising processing of 3-D GPR data, so it is urgent to further explore the efficient denoising algorithm of 3-D GPR data [45], [46].

The time cost of dataset construction and network training in the denoising method based on deep learning is nonnegligible, and the application scenarios are usually limited to 2-D. With the development of a sparse representation algorithm, the adaptive learning dictionary algorithm compared with fixed basis transformation also shows a strong ability in geophysical data processing. Many scholars achieved the 2-D/3-D seismic data denoising [47], [48], [49] by efficient dictionary learning. Feng et al.'s [50] research confirms the feasibility of the K-SVD algorithm for Gaussian noise and clutter removal in 2-D GPR data. However, the main disadvantage of the K-SVD is that it needs to perform a multitude of SVD, as mentioned above, which results in unacceptable computational efficiency, especially in practical multidimensional problems. Aiming at this problem, Sahoo and Makur [51] proposed a sequential generalized K-means (SGK) algorithm and verified its high efficiency in image denoising [52]. SGK algorithm also has wonderful performance in multidimensional seismic signals denoising [49] and missing trace reconstruction [53].

In this article, to evaluate the performance and efficiency of the proposed SGK algorithm for complex multidimensional data, three sets of experiments for 3-D GPR data were carried out. Under the same computing resources, the calculation time and denoising effect of the two methods are compared in each group of experiments. The principles of K-SVD and SGK algorithm are analyzed mathematically in Section II. Then, K-SVD and SGK methods are used to suppress random noise and clutter interference of 3-D GPR data, and the results are compared in Sections III and IV. In Section V, we draw a conclusion that the SGK algorithm is an efficient 3-D adaptive denoising method.

II. Method

Sparse representation is to represent a natural signal by linear superposition of a set of basis vectors, which belongs to an unsupervised algorithm [54]. The sparse representation of the signals needs to achieve the two goals of sparse coding and dictionary learning, and these two steps are calculated alternately until the end of the iterative calculation [55].

A. Sparse Coding

In the sparse representation model, the observed data Y can be expressed as

$$\min \|X\|_0 \text{ s.t. } Y = DX \quad (1)$$

where X is the sparse coding coefficient, and $\| \|_0$ is the l_0 norm, its value is the number of nonzero elements of a vector in X. The sample set Y ($N\times M$) is represented by M column vectors y_i ($N\times 1$). The dictionary matrix D ($N\times K$) is composed of K signal-atoms for columns, d_i ($N\times 1$). It is assumed that Y can be reconstructed by linear multiplying the dictionary D and the sparse coefficient X. When $K > N$, D is called an overcomplete dictionary, which leads to the unique solution of the linear equation. To find the optimal solution X, we introduce the constraints:

$$\forall_i \mathbf{x}_i^n = \arg\min_{\mathbf{x}_i} \|Y - D^n X\|_F^2 \text{ s.t. } \forall i \|x_i\|_0 \leq T_0 \quad (2)$$

T_0 is a constant, called sparsity constraint threshold. There are two variables D and X to be optimized. In the sparse coding stage of dictionary learning, the main goal is to calculate the sparse coefficients X based on a given signal Y and the fixed dictionary D. However, the exact rigorous solution of sparsest representations is an NP-hard problem [32], so we have to choose the orthogonal Matching Pursuit (OMP) algorithm [56] to calculate the approximate solution of sparse coefficients. In the first sparse coding calculation, we use the DCT dictionary in the fixed dictionary as the initial dictionary.

B. Dictionary Update via K-SVD

In the dictionary update stage, the K-SVD algorithm uses a column-by-column update method, the sparse coefficient X j is fixed, and any dictionary atom d_k is selected in order in dictionary D_j for update calculation. The calculation objective function can be expressed as

$$\begin{aligned}\|Y - DX\|_F^2 &= \left\| Y - \sum_{j=1}^{L} d_j x_T^j \right\|_F^2 \\ &= \left\| \left(Y - \sum_{j \neq k} d_j x_T^j \right) - d_k x_T^k \right\|_F^2 \\ &= \left\| E_k - d_k x_T^k \right\|_F^2 . \end{aligned} \tag{3}$$

The kth row vector of X corresponding to d_k is $x^k{}_T$. The error matrix generated by the fitting of the column vector d_j except d_k and its corresponding coefficient row vector x_j is defined as E_k. Now, our optimization problem can be modified into

$$\min_{d_k, x_T^k} \| E_k - d_k x_T^k \|_F^2 . \tag{4}$$

We use the SVD algorithm to carry out the update process, find the matrix $d_k \times x^k{}_T$ with the minimum distance from E and the rank of 1 to obtain the optimal solution d_k. However, if E_k is directly decomposed by SVD, the updated $x^k{}_T$ will be not sparse, resulting in d_k unsatisfying the sparse condition, so we define the index set $\omega_k = \{i | 1 \leq i \leq M, \mathbf{x}_T^k(i) \neq 0\}$, and let Ω_k represent a matrix of size $N \times |\omega_k|$, the number at ($\omega_k(i)$, i) is 1, and the other positions are 0. By multiplying (4) by a nonzero limiting factor Ω_k, the result is as follows:

$$\left\| E_k \Omega_k - d_k x_T^k \Omega_k \right\|_F^2 = \left\| E_k^R - d_k x_R^k \right\|_F^2 . \tag{5}$$

At present, the new matrix E_k^R can be directly decomposed by SVD

$$E_k^R = U \Sigma V^T . \tag{6}$$

The first column vector of the left singular matrix U is set as d_k, and the multiplication of the first column vector of the right singular matrix V and the first singular value $\Sigma(11)$ is taken as $x^k{}_R$. After getting $x^k{}_R$, update it to the original $x^k{}_T$. So far, the update of the kth column atom in the dictionary has been completed. Next, we update D_j column by column until the last dictionary atom calculations are completed to form a new dictionary D_{j+1}, and then the cycle is performed once to solve X in (2).

C. Dictionary Update via SGK

K-SVD is widely used in sparse representation, but the existence of massive SVD calculations hinders its application in complex multidimensional problems. Therefore, the SGK dictionary learning algorithm is proposed to improve computational efficiency. The objective function of SGK can be expressed as

$$\forall_i x_i^n = \arg\min_{\mathbf{x}_i} \|Y - D^n X\|_F^2 \text{ s.t. } \forall_i x_i = e_p \tag{7}$$

where e_p is the unit vector, p denotes the pth element of x_i that is 1, and the remaining elements are all 0. In terms of constraints on the coefficient vector, the K-SVD algorithm uses the sparsity constraint expressed in (2). The difference is that in the SGK algorithm, the coefficient vector is the unit vector. The constraint of this special structure means that for the calculation of the optimal sparse coefficient, the number of sparse coding calculations is reduced from p to 1, with a decrease in the sparse coding process time. According to the derivation of (5), the objective function is defined as

$$J = \left\| E_k^R - d_k x_R^k \right\|_F^2 \tag{8}$$

different from the K-SVD algorithm, which uses SVD to minimize the objective function, the SGK algorithm chooses the least square method to solve the problem. First, we calculate the derivative of J with respect to d_k, and set the result to 0

$$\frac{\partial J}{\partial d_k} = -2 \left(E_k^R - d_k x_R^k \right) \left(x_R^k \right)^T = 0 \tag{9}$$

solving (9) leads to

$$d_k = E_k^R \left(x_R^k \right)^T \left(x_R^k \left(x_R^k \right)^T \right)^{-1} . \tag{10}$$

The above formula can further be expressed as

$$\begin{aligned} E_k^R \left(x_R^k \right)^T &= \left(Y_R - \sum_{i \neq k} d_k x_R^i \right) \left(x_R^k \right)^T \\ &= Y_R \left(x_R^k \right)^T + \sum_{i \neq k} d_k x_R^i \left(x_R^k \right)^T . \end{aligned} \tag{11}$$

The meaning of Y_R is the same as Y in (3) but the selection set ω_k selects all the nonzero elements in $x^k{}_T$, so its size is smaller than Y. Since $\forall_i$, $||x_i||_0 = 1$, as constrained by (7), we can get the formula

$$\forall_{i \neq k} x_R^i \left(x_R^k \right)^T = 0 \tag{12}$$

where $x^k{}_M$ is a smaller version of the row vector $x^k{}_T$ and all of its elements are 1, and Y_R $(x^k{}_R)^T$ can be written as the sum of all column vectors of Y_R

$$Y_R \left(x_R^k \right)^T = \sum_{i \in \omega_k} y_i \tag{13}$$

supposing that there are $N^k{}_r$ nonzero elements in the row vector $x^k{}_M$, then

$$x_R^k \left(x_R^k \right)^T = N_r^k \tag{14}$$

according to formulas (13) and (14), (10) can be written as

$$d_k = \frac{\sum_{i \in \omega_k} y_i}{N_r^k}. \tag{15}$$

Equation (15) is the updating formula of the kth atom in dictionary D. In the process of dictionary updating, the SVD operation with a huge amount of calculation shown in (6) is replaced by the simple summation of training samples in the SGK algorithm. Therefore, SGK has become a more efficient sparse representation calculation method than K-SVD. Next, we will use several experiments to verify the performance of the two dictionary learning methods.

III. Numerical Experiments

Due to the environmental interference, the limitation of hardware equipment and the inhomogeneity of the underground medium, the GPR data not only includes the reflected wave of the underground target but also various noise and interference waves. Data with noise can be modeled as $dn = d + n$, where dn denotes the noisy observed data, d is noise-free raw data, and n represents the noises, respectively. We set up comparative experiments on the results of denoising 3-D synthetic data and field data. In the case of known original clean data, the data noise level is quantified by signal-to-noise ratio (SNR). The calculation formula is as follows:

$$\textbf{SNR} = 10 \log_{10} \frac{\|d\|_2^2}{\left\|d - \hat{d}\right\|_2^2}. \tag{16}$$

Larger SNR proves a lower noisy level. The normalized mean-square error (NMSE) is selected to represent the denoising performance. The smaller NMSE value represents a better denoising result.

$$\textbf{NMSE} = \frac{\left\|d - \hat{d}\right\|_2^2}{\|d\|_2^2} \tag{17}$$

where $\hat{d}$ represents the noisy data or processed data.

A. Random Noise in Homogeneous Medium

A simulated layered model with the region of 0.4 × 1.6 × 0.8 m based on real road structure is established as Fig. 1. In the asphalt layer, cracks with a depth of 0.10 m, a width of 0.02 m, and a length of 0.4 m are set throughout the entire asphalt layer. At the junction of the cement layer and the soil layer, due to the subsidence of the soil layer, an irregular cavity with a radius of about 0.04 m appears at the junction. The center of the irregular cavity is located underground (1 m, 0.2 m, 0.35 m). Both anomalous bodies are filled with air, that is, the relative dielectric constant is set to 1, and the conductivity is set to 0.

The discrete mesh size is 40 × 160 × 80, with a mesh interval of 0.01 m, and the 15-layer conductive perfectly matched layer is used as the absorption boundary. The Ricker wavelet with a main frequency of 900 MHz is placed on the surface as a pulse source. The simulation time window is 12 ns, the sampling interval is 0.01 ns, the transceiver distance is 0.08 m, and the channel spacing is 0.02 m. A total of 74 channels of data are recorded and 20 survey lines are laid in the Y-direction. The forward method we choose is the finite-difference time-domain algorithm. The forward result is obtained in Fig. 2(a). By adding Gaussian noise with a mean value of 0 and a standard deviation of 30 to the original data, the noise-added forward result is shown in Fig. 2(d). The SNR of the noisy image obtained by (16) is 18.11 dB. The Gaussian noises make the profile messy and interfere with the subsequent processing and interpretation of the data. For the purpose of testing the denoising effect, the K-SVD and SGK denoising algorithms are used in the noise-added forward data, respectively. The data size of the forward result of the above-mentioned model is 20 × 74 × 1200, and the selected atomic block size is 4 × 4 × 4, with a total of 64 atoms. The moving step size of the 3-D atom block in each direction is set to be 2. In this case, the size of the sample signal d is 64 × 194 076. The denoising results shown in Fig. 2(b) and (c) illustrate that the noise and the effective wave are separated perfectly, and the reflected wave in the profile is intact and clear. Fig. 2(e) and (f) shows the random noises removed by the two methods, respectively. And the parameter distribution of the 3-D road simulation model is listed in Table I. There are some effectively reflected waves with the same arrival time as the direct wave in the denoising residual but this hardly affects the overall denoising effect of the algorithm.

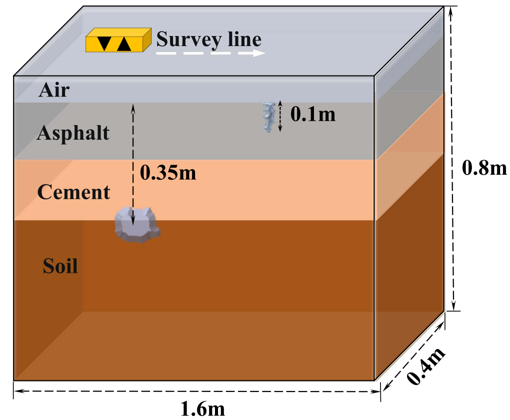

Fig. 1. 3-D road simulation model.

TABLE I
Parameter Distribution of Road Model

Media types	Thickness (m)	ε_r	σ
Air	0.50	1	0
Asphalt	0.15	4	3
Cement	0.20	6	5
Soil	0.40	12	10

The SNR of the noisy image is greatly improved by the two algorithms, and the NMSE is reduced by an order of magnitude. The calculation speed SGK is about eight times higher than that of K-SVD in the case of ensuring the denoise effect, as given in Table II. Observing the A-Scan data in Fig. 3, the waveform of

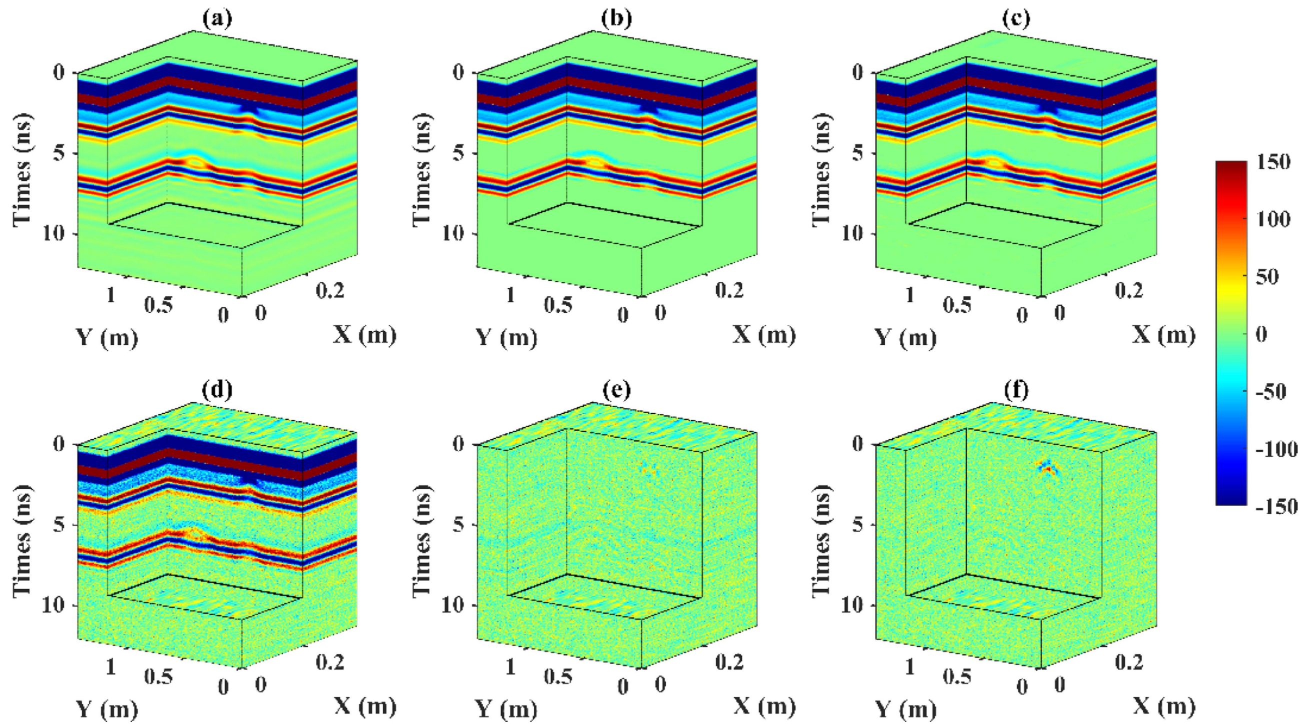

Fig. 2. 3-D synthesis example of homogeneous media. (a) Clean data. (b) Denoised data by K-SVD. (c) Denoised data by SGK. (d) Noisy data. (e) Noise removed by K-SVD. (f) Noise removed by SGK.

TABLE II
COMPARISON OF DENOISING RESULTS OF THE K-SVD AND SGK (BOLD) METHODS FOR HOMOGENEOUS MEDIUM MODEL

	Time (s)	SNR	NMSE
Noisy data	-	18.11	0.0155
K-SVD	455.15	24.19	0.0038
SGK	**57.40**	23.53	0.0041

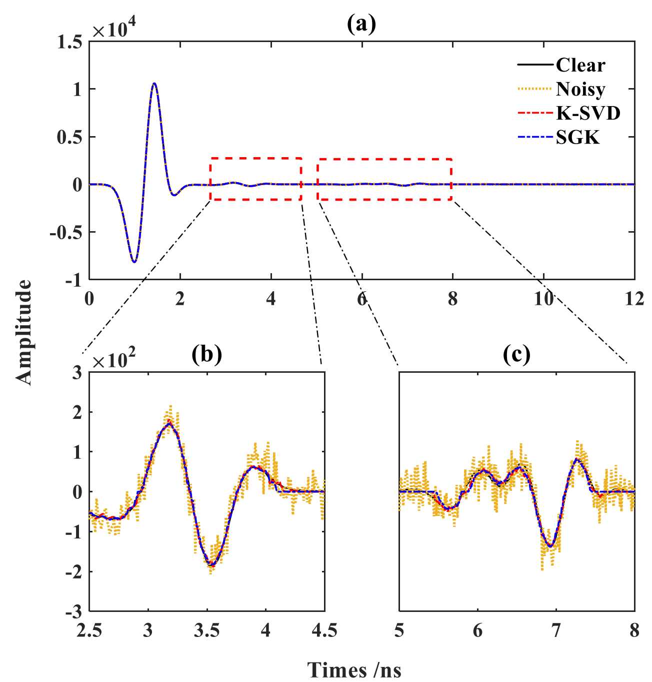

Fig. 3. (a) Overall situation. (b) Partial enlargement of data from 2.5 to 4.5 ns. (c) Partial enlargement of data from 5 to 8 ns.

the reflected wave after denoising by the K-SVD dictionary and the SGK dictionary corresponds well to the original data, and the data are basically on the same amplitude. It can be concluded that the denoising effects of the two methods are prosperous since the SGK algorithm updates the dictionary atoms by the arithmetic means of the training signal, and the accuracy is partially reduced compared with the K-SVD algorithm while improving the calculation speed.

In the learning process, the atomic blocks overlap each other, so the block-based representation is highly redundant. This overlapping technique and highly redundant representation are crucial to the denoising effect. Compared with the K-SVD method, the main difference of SGK is the method of dictionary updating. The dictionary after learning is reshaped into a 2-D matrix with an atom size of 8×8, and each dictionary has a total of 64 atoms. The first eight atoms of the three dictionaries are taken as a 3-D example. Comparing Fig. 4(b) and (c) with (a), the sparse coefficient distribution of the learning dictionary is not completely random but has a certain regular redundant structure, and there is a strong local self-similarity. The atoms of K-SVD are more structural; in contrast, the SGK algorithm has the rules of updating the atoms to take the average number of data, which makes the atomic structure messier and less regular.

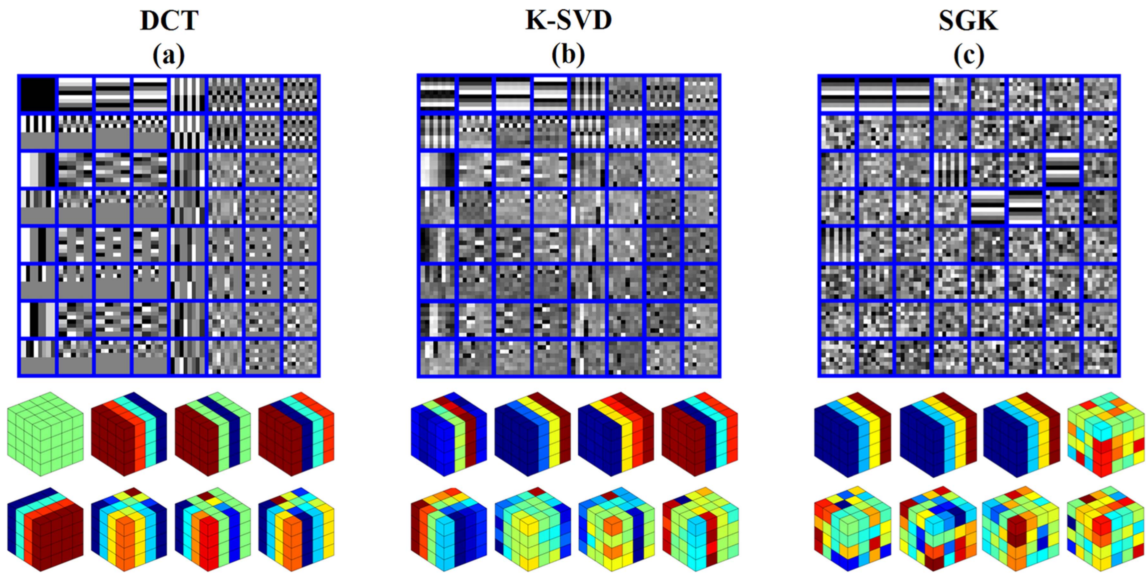

Fig. 4. 2-D and 3-D display and comparison of different dictionary atoms.

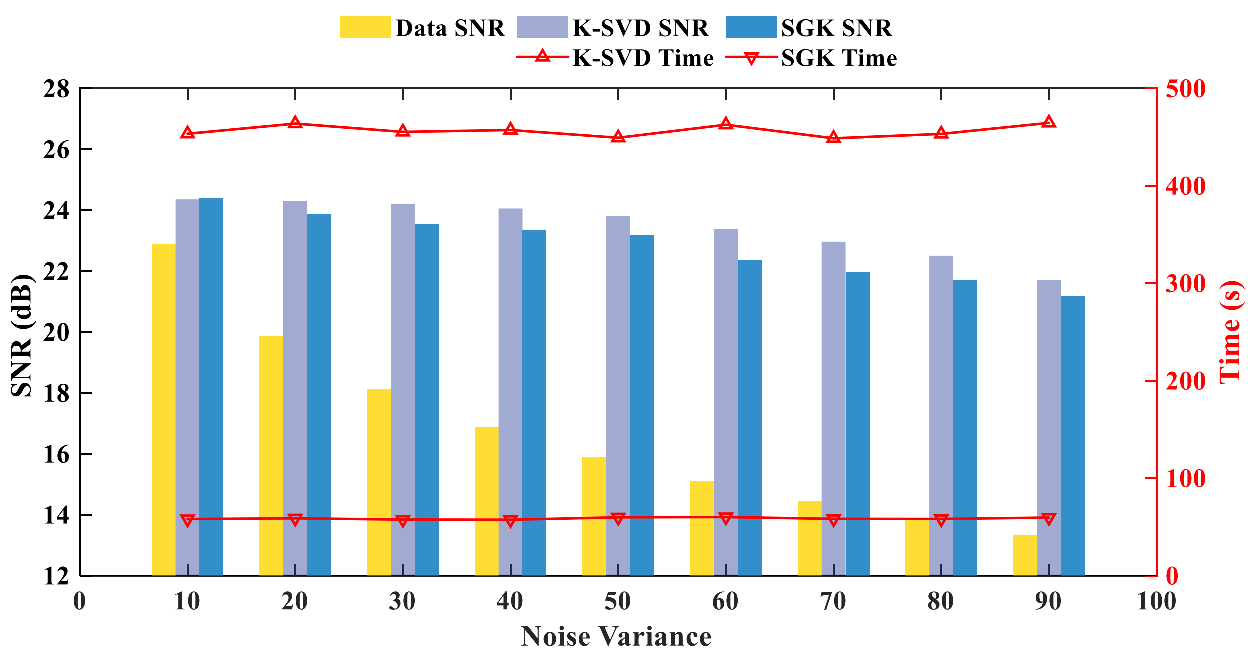

Fig. 5. Comparison of the SNR and time consumption of each denoising result by K-SVD and SGK methods with the increase of noise variance.

To further explore the denoising performances of the two methods and the speed improvement of the SGK algorithm, the comparative experiments of the two methods at different noise levels and under different size models are carried out. To compare the calculation time fairly, each of the following examples is repeated three times under the same computing, and the three times average is taken as the final result.

The change of the output SNR with the different input SNR resources is illustrated in Fig. 5 shows when the noise variance is 10, the denoising effect of the K-SVD method and the SGK method is almost the same. In other cases, the removal effect of the K-SVD algorithm with random noise is slightly better than that of SGK. With the decrease in the input SNR, the output SNR of both algorithms is maintained above 20 dB, which proves the superiority of the dictionary learning denoising method in a low SNR. In the meantime, for the data of the same size, the calculation time of SGK is almost the same, while K-SVD has a certain fluctuation. The SGK method is much faster than the K-SVD algorithm under the same computing resources, and the computational efficiency has been maintained at about 7.5×. Table III lists the time-consuming comparison of the algorithm under the same calculation conditions when processing data of different scales. With the increase in data size, the calculation speed of SGK is still about 7.5× faster than K-SVD. Therefore,

TABLE III
COMPARISON OF COMPUTATIONAL COST OF THE K-SVD AND SGK (BOLD) METHODS FOR DIFFERENT DATA SIZES

Data size	1200×75×20	1200×75×100	1200×75×200
K-SVD	455.15	2480.28	4989.55
SGK	**57.40**	**321.18**	**655.19**

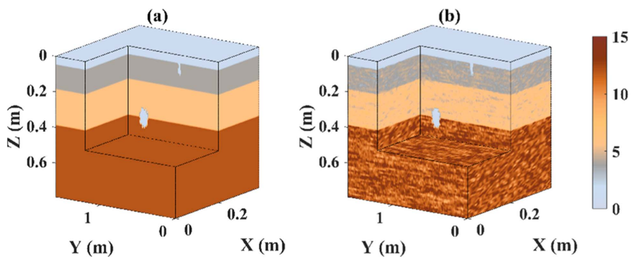

Fig. 6. Diagram of the road simulation model. (a) Homogeneous medium. (b) Random medium.

the SGK algorithm has a great efficiency advantage in processing massive 3-D GPR data.

B. Clutter Interference in Random Media

In the actual detection, because the underground material is not evenly distributed, the electromagnetic wave propagates in the medium with complex distribution, which will produce a lot of scattering and diffraction so that there is substantial clutter interference in the reflection profile, affecting the depth and accuracy of exploration, influencing interpretation. Therefore, we adapt an exponential elliptic autocorrelation function to construct a random medium model to consider the performance of dictionary learning for clutter removal, and the function expression is

$$\phi(x, y, z) = \exp\left[-\sqrt{\left(\frac{x^2}{a^2} + \frac{y^2}{b^2} + \frac{z^2}{c^2}\right)}\right] \quad (18)$$

where a, b, and c represent the autocorrelation length of the medium in the x, y, and z directions, respectively. Fig. 6(b) is a road simulation model of the random medium, in which the autocorrelation length $a = b = c = 0.1$ m, the variance is 0.1, the mean value is the background medium value, and the other model parameters are consistent with the parameters of the homogeneous medium model.

Fig. 7(c) is the forward section of the random medium model. The clutter that affects the identification of effective signals is removed by dictionary learning, and the homogeneous medium forward data are used as the original noise-free data.

The selected atomic block size is $4 \times 4 \times 4$, with a total of 64 atoms of two denoising algorithms. The moving step size of the 3-D atom block in each direction is set to be 2. Fig. 7 shows that both dictionary denoising algorithms complete the perfect separation of clutter and effective wave. It can be seen intuitively from the comprehensive Fig. 8 and Table IV that both

TABLE IV
COMPARISON OF THE DENOISING RESULTS OF THE K-SVD AND SGK (BOLD) METHODS FOR RANDOM MEDIUM MODEL

Algorithm	Time(s)	SNR (dB)	NMSE
Clean data	-	19.72	0.0107
K-SVD	450.47	20.97	0.0080
SGK	**60.19**	**20.53**	**0.0088**

methods have a good suppression effect on clutter, and the SGK algorithm improves the calculation speed by 7.5× compared with the K-SVD algorithm while ensuring the denoising effect.

C. Field Data Experiment

The field data were acquired from the southwest side of the water purification plant in the east district of Huangpu District, Guangzhou City. The water engineering construction is laid along the current Hongguang Road, and the new pipe jacking length was 113 m. To find out whether there are road diseases in the pipe jacking pipeline after the construction of the pipe jacking project of the water conservancy project, and to eliminate the potential safety hazard of ground collapse, the Italian 3-D GPR (Stream X) is used to ascertain the underground situation.

The central frequency is 200 MHz, and the sampling time is 80 ns. Three wire harnesses with a length of 0.113 km are arranged to achieve full coverage measurement, and the detection workload is 0.339 km. We selected the 3-D field GPR data with a size of $512 \times 400 \times 14$, as shown in Fig. 9(a), for denoising experiments. It can be found that the underground medium is unevenly distributed, the horizon information is rich, the clutter reflection is excessive, and the high-frequency noise in the deep is intense, which influences the processing and interpretation of the effective wave.

The selected atomic block size is $4 \times 4 \times 4$, a total of 125 atoms. The moving step size of the 3-D atom block in each direction is set to be 2. Therefore, in this example, the size of the sample signal d is $125 \times 304\,470$. The comprehensive Figs. 9 and 10 demonstrate that both dictionary learning methods effectively eliminate random noise and clutter, resulting in a significant improvement of the SNR. The fifth profile of the field data is visually compared through a 2-D display to evaluate the denoising results. The corresponding outcomes are illustrated in Fig. 9(d)–(f) as well as in Fig. 10(c) and (d). The loss of effective waves is negligible, and the denoising effects of the two methods are almost the same. Moreover, the K-SVD algorithm takes 1357.50 s, while the SGK only takes 167.74 s, and the speed is increased by nearly eight times.

The 3-D GPR data can provide views in three directions: vertical section, horizontal plane, and cross section. The acquired data contain abundant information. To examine the changes in the horizontal slices crucial for interpreting 3-D radar data after denoising, we conducted C-Scan demonstrations. Four consecutive horizontal slices at different travel times are selected, as shown in Fig. 11(a). By observing the results and residuals of

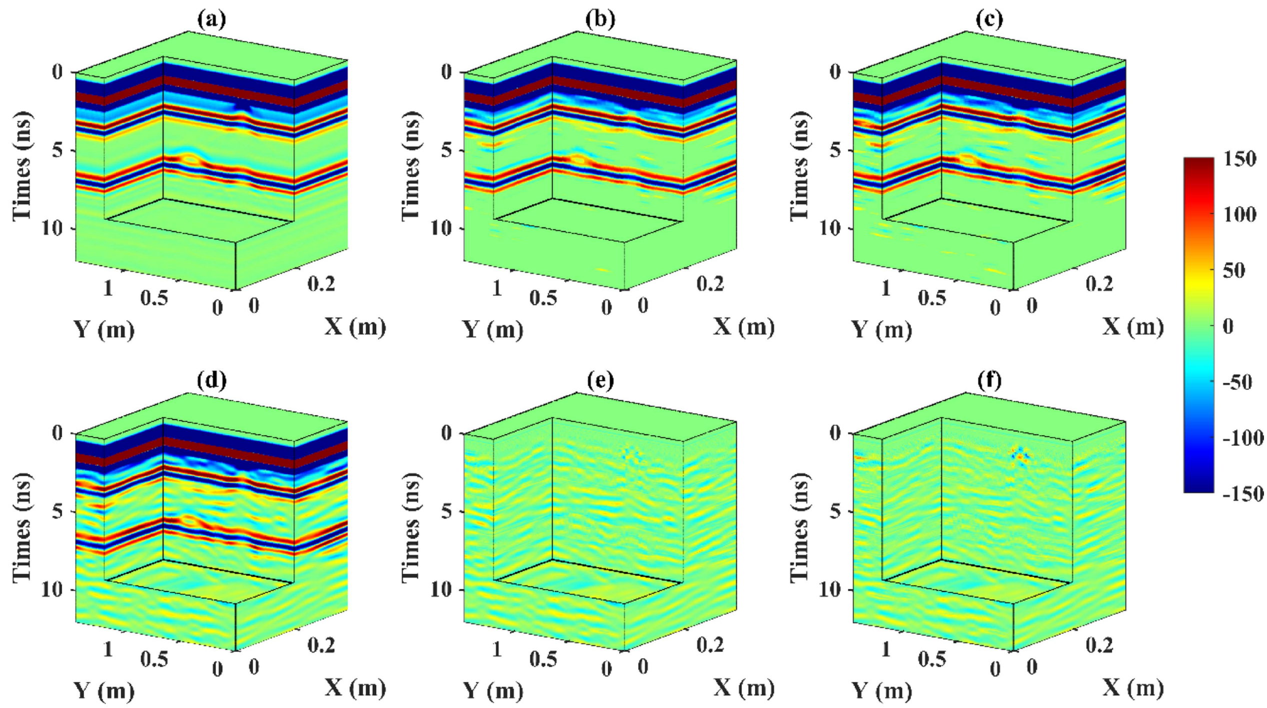

Fig. 7. 3-D synthesis example of the random medium. (a) Forward data of homogeneous medium (clean data). (b) Denoised data by K-SVD. (c) Denoised data by SGK. (d) Forward data of random medium with clutter (noisy data). (e) Noise by K-SVD. (f) Noise by SGK.

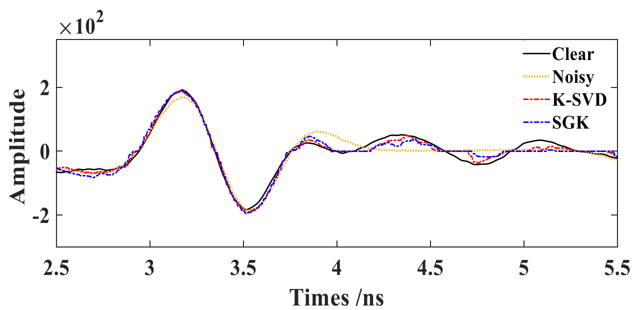

Fig. 8. Local amplification from 2.5 to 5.5 ns of random medium forward data denoising results.

the SGK algorithm denoising processing shown in Fig. 11(b) and (c), it is evident that clutter interference in the reflection profile is reduced, ensuring clear and continuous variations of target hyperbolic reflected waves in the horizontal direction, thus guaranteeing accurate subsequent GPR data interpretation. Furthermore, we selected three continuous horizontal slices near 63 ns, as shown in Fig. 11(d). The presence of deep high-frequency noise obstructed the observation of variation characteristics in reflected waves horizontally. In Fig. 11(e) and (f), the reflection profile became complete and distinct with more apparent trends in reflection wave changes observed. The signals within residual data profiles exhibited discontinuity with low amplitude consistent with noise characteristics.

In Fig. 12, the atomic representations of the two dictionaries are highly redundant and contain a large amount of data structure information. Using this as prior information to denoise the data will enhance the completeness of the atom, making the sparse representation more reasonable and accurate, thereby improving the quality of the signal in the complex area. Observing the 3-D display of the first 16 dictionary atoms, the structure information of the K-SVD algorithm dictionary is more complex.

To observe the denoising results more intuitively, we selected the A-scan at the 328th signal of the 10th profile and the spectrum analysis is carried out by short-time Fourier transform (STFT). As can be seen from Fig. 13, the denoising method effectively suppresses the high-frequency oscillation interference in the deep part, and the denoising result of the SGK algorithm is smoother, which also leads to the loss of some effective signals. The spectrum analysis results intuitively show that the central emission frequency of the data acquisition is 200 MHz, and the amplitude of the deep effective signals with high-frequency noise is small. By analyzing the STFT results in Fig. 13(b)–(d), we can figure out that both algorithms can effectively suppress high-frequency noise; in contrast, the removal effect of K-SVD on high-frequency noise is slightly inferior to the SGK, but the damage of SGK to deep effective signals is more tremendous. In general, both algorithms can effectively remove noise, and the calculation speed of the SGK algorithm is about eight times that of the K-SVD algorithm.

IV. Discussion

The classical K-SVD dictionary learning method is limited in its application to complex high-dimensional problems due to the requirement of multiple SVD calculations. Therefore, we propose the SGK efficient dictionary learning algorithm for denoising 3-D GPR data. In this algorithm, called SGK, the dictionary atoms are updated through the arithmetic mean of

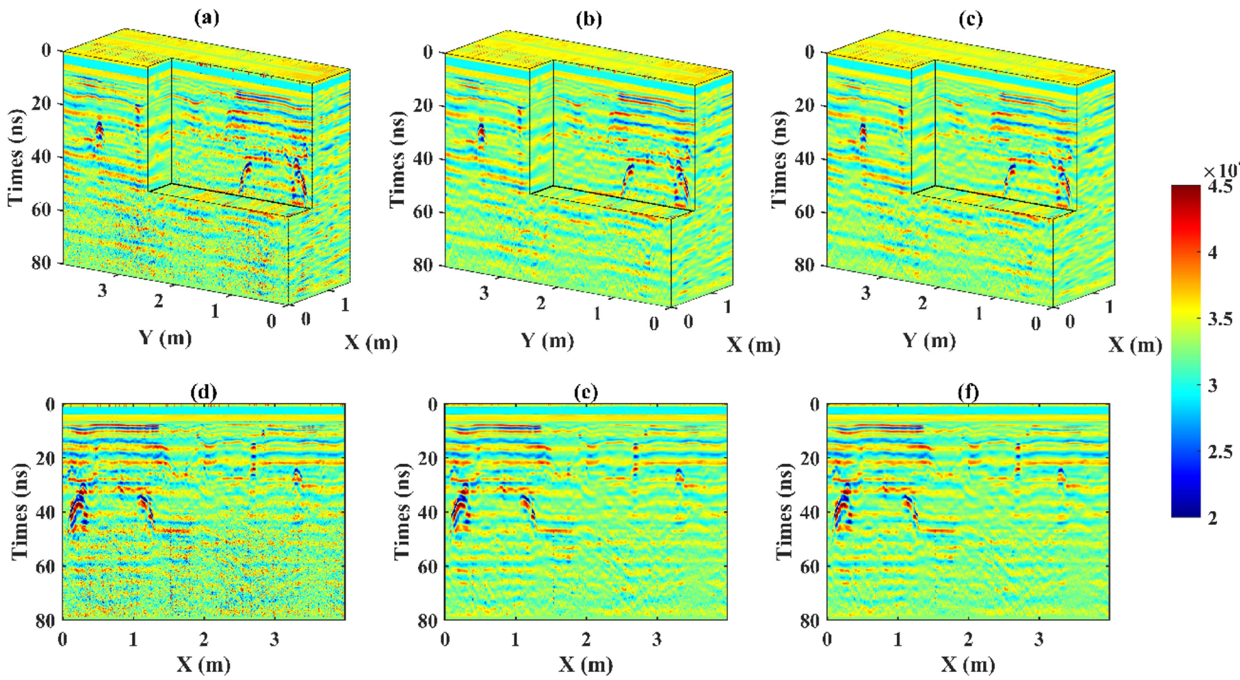

Fig. 9. 3-D field data and denoising results. (a) Field data. (b) Denoised data by K-SVD. (c) Denoised data by SGK. (d) 2-D profile of the field data. (e) 2-D profile of the K-SVD. (f) 2-D profile of the SGK.

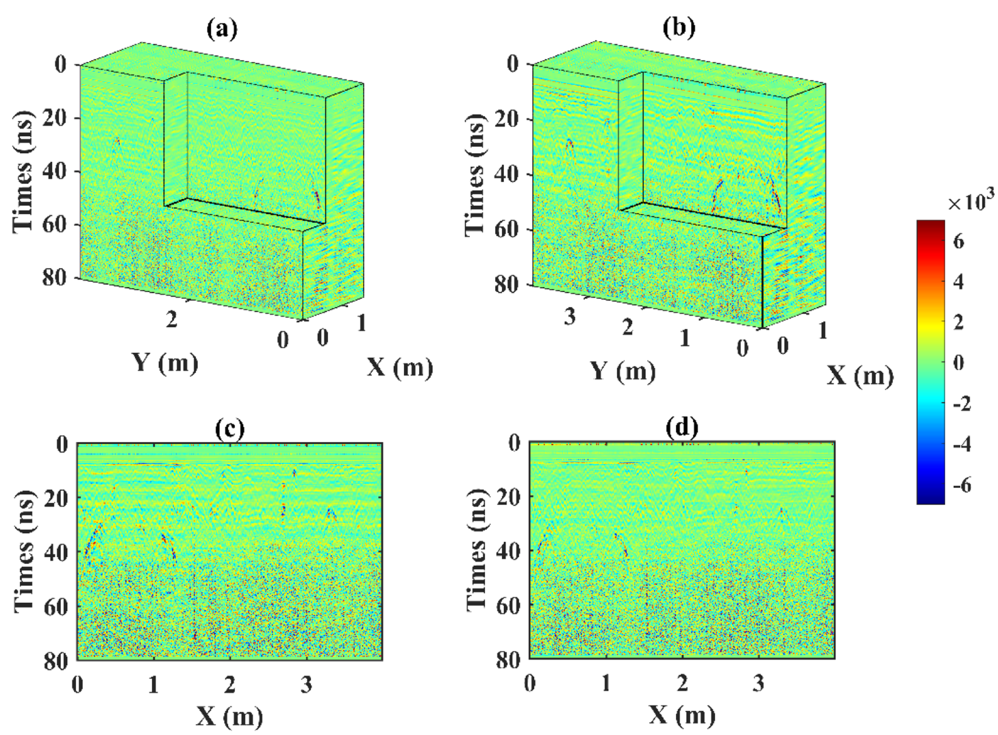

Fig. 10. Removed noise. (a) Noise removed by K-SVD. (b) Noise removed by SGK. (c) 2-D profile of the K-SVD noise. (d) 2-D profile of the SGK noise.

multiple training signals, which eliminates the need for numerous time-consuming SVD calculations. Both dictionary learning algorithms demonstrate excellent performance in removing random noise and clutter interference from 3-D GPR data. Compared with the K-SVD algorithm, SGK achieves a more than 7.5× increase in calculation speed while slightly sacrificing denoising effectiveness. Consequently, the fast dictionary learning algorithm SGK holds great potential for addressing high-dimensional geophysical problems. When employing dictionary learning algorithms, designing appropriate atoms is a crucial factor that affects both denoising effectiveness and efficiency. We take the 3-D forward data of the random medium as an

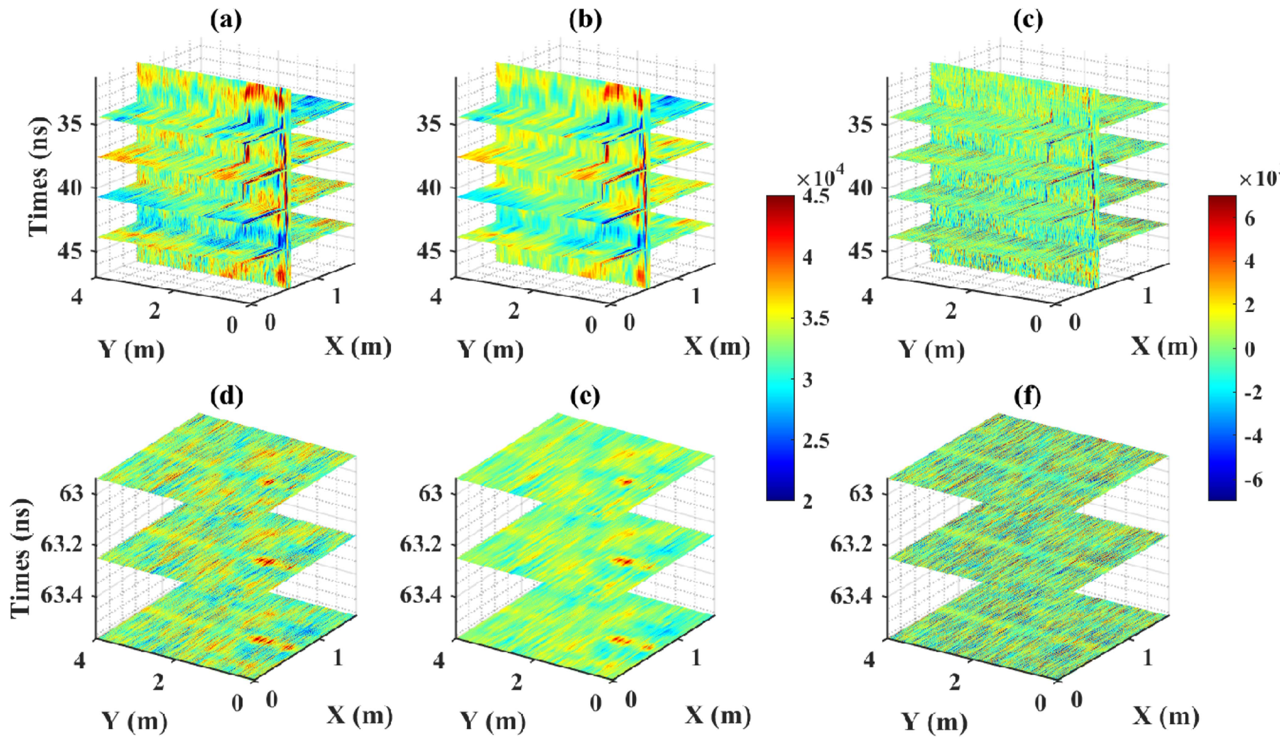

Fig. 11. C-Scan near 40 ns and 63 ns of the field data and its denoising results. (a) Field data. (b) Denoised data by SGK. (c) Noise removed by SGK. (d) Field data. (e) Denoised data by SGK. (f) Noise removed by SGK.

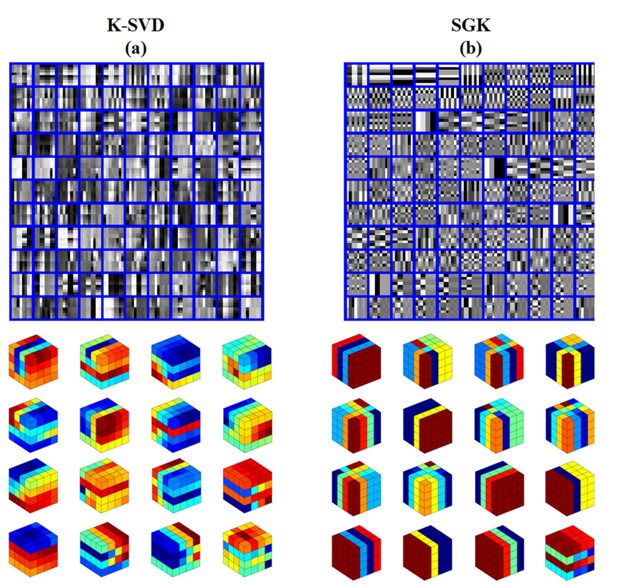

Fig. 12. 2-D and 3-D display and comparison of different dictionary atoms.

example to discuss the parameter selection principle of the SGK algorithm.

The SNR and NMSE of the synthetic data are 19.72 and 0.0107, respectively. To discuss the selection of parameters such as the number, size, and step size of atoms in dictionary learning, we conducted four sets of comparative experiments for each parameter, and finally determined the optimal parameters. Each group of experiments was repeated three times under identical conditions, and the average value from these repetitions was considered as the final result. When discussing the parameters, we solely focused on the proposed method; hence, all aforementioned experiments were denoised using the SGK algorithm. Based on the input 3-D GPR data's dimensions, we needed to select appropriate values for k (number of atoms), l (size), s (moving step size), and other relevant parameters to achieve optimal denoising effect. By employing a controlled variable approach, three groups of experiments were designed with their results presented in Tables V–VII. The optimum results in the three groups of experiments were boldly labeled respectively.

TABLE V
DENOISING RESULTS AND CALCULATION TIME OF DIFFERENT k (l=4, s=2)

k	SNR	NMSE	Time (s)
49	20.44	0.0092	54.52
64	**20.53**	**0.0080**	**60.19**
100	20.26	0.0094	98.89
125	20.10	0.0098	123.71

Currently, there is no established standard for selecting parameters such as the number and size of atoms. The selection process primarily relies on the dimensions and structure of the input data, guided by empirical values. From the aforementioned experiments, it can be observed that when atoms are small in number and size, the learning of data structures remains incomplete, resulting in a higher presence of noise residues.

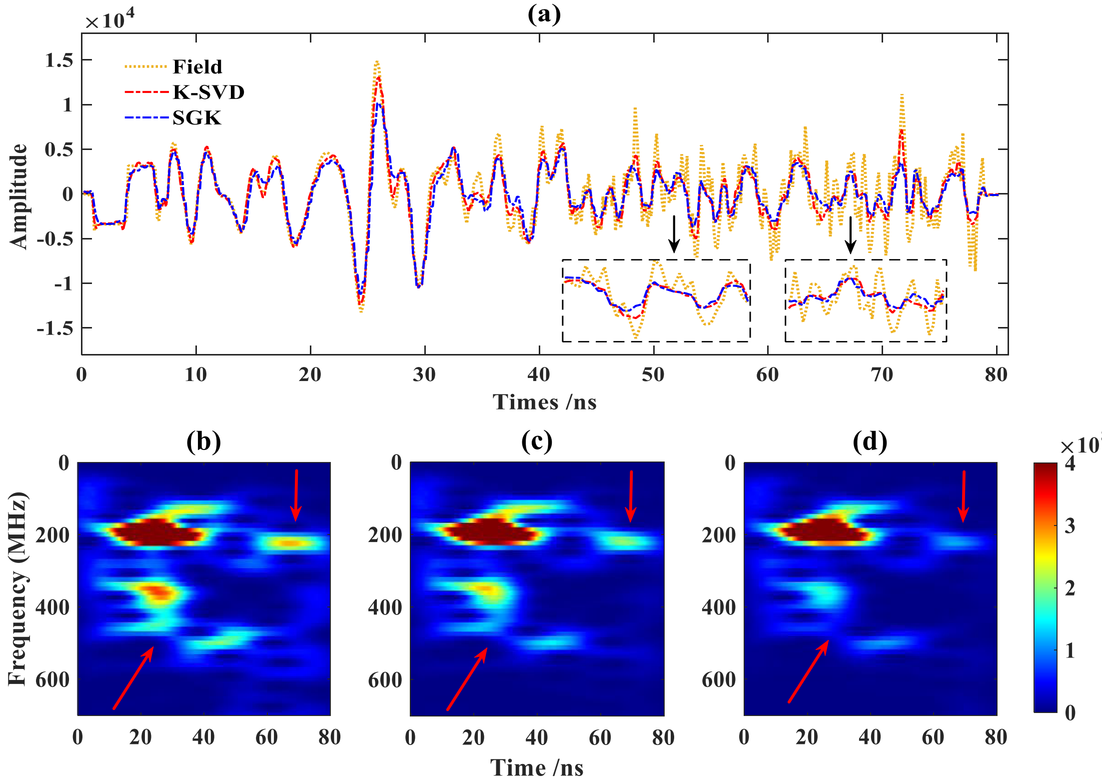

Fig. 13. Comparison of field data denoising results. (a) A-scan comparison. (b) STFT of the filed data. (c) STFT of the denoised data using K-SVD. (d) STFT of the denoised data using SGK.

TABLE VI
DENOISING RESULTS AND CALCULATION TIME OF DIFFERENT L (K=64, S=2)

l	SNR	NMSE	Time (s)
2	19.92	0.0102	64.26
3	18.54	0.0140	76.62
4	**20.53**	**0.0080**	**60.19**
5	12.92	0.0510	83.48

TABLE VII
DENOISING RESULTS AND CALCULATION TIME OF DIFFERENT S (K=64, L=4)

s	SNR	NMSE	Time (s)
1	21.02	0.0079	513.78
2	**20.53**	**0.0080**	**60.19**
3	16.44	0.0227	25.15
4	10.57	0.0877	10.42

Conversely, if atoms are excessively large in number and size, they may impair effective signal detection by reducing SNR while significantly increasing computational time. In addition, the step size for atomic movement exerts a substantial influence on both calculation results and time; hence, parameter selection should align with input data dimensions. The optimal parameters vary for different input data, necessitating further investigation into the integration of deep learning to enhance the automation of parameter selection and achieve true adaptability in dictionary learning algorithms.

V. Conclusion

Aiming to address the issue of multidimensional GPR data processing, three sets of data denoising experiments were conducted, yielding the following conclusions.

1) The performance of both methods in eliminating random noise is nearly identical, with K-SVD slightly outperforming SGK. As the input SNR of the forward modeling results decreases from 23 to 14 dB, the output SNR of the two algorithms is maintained above 20 dB, demonstrating that the dictionary learning denoising method excels at low SNR conditions.
2) Both dictionary algorithms effectively leverage prior information from sample data and adaptively extract features for removing random noise and clutter interference during 3-D GPR field data processing applications, which holds significant practical implications.
3) In comparison, it can be observed that the denoising effect achieved by the SGK dictionary algorithm is comparable to that of K-SVD while maintaining an operation acceleration ratio exceeding 7.5×. Thus, the SGK dictionary learning algorithm proves to be an efficient approach for multidimensional data processing.

ACKNOWLEDGMENT

The authors would like to thank the Editors for their invaluable guidance in implementing this study. They also extend their appreciation to the anonymous reviewers for providing constructive comments and suggestions that significantly enhanced the previous version of this article. Other special detection cases are available by contacting the authors.

REFERENCES

[1] H. Liu, K. Takahashi, and M. Sato, "Measurement of dielectric permittivity and thickness of snow and ice on a brackish lagoon using GPR," *IEEE J. Sel. Topics Appl. Earth Observ. Remote Sens.*, vol. 7, no. 3, pp. 820–827, Mar. 2014.

[2] D. Comite, A. Galli, S. E. Lauro, E. Mattei, and E. Pettinelli, "Analysis of GPR early-time signal features for the evaluation of soil permittivity through numerical and experimental surveys," *IEEE J. Sel. Topics Appl. Earth Observ. Remote Sens.*, vol. 9, no. 1, pp. 178–187, Jan. 2016.

[3] S. Santos-Assunçao et al., "GPR backscattering intensity analysis applied to detect paleochannels and infilled streams for seismic nanozonation in urban environments," *IEEE J. Sel. Topics Appl. Earth Observ. Remote Sens.*, vol. 9, no. 1, pp. 167–177, Jan. 2016.

[4] S. X. Liu, Q. Lu, H. Q. Li, and Y. X. Wang, "Estimation of moisture content in railway subgrade by ground penetrating radar," *Remote Sens.-Basel*, vol. 12, no. 18, Sep. 2020, Art. no. 2912.

[5] T. X.-H. Luo and W. W. L. Lai, "Subsurface diagnosis with time-lapse GPR slices and change detection algorithms," *IEEE J. Sel. Topics Appl. Earth Observ. Remote Sens.*, vol. 13, pp. 935–940, 2020.

[6] X. Zhou, Q. Chen, S. Lyu, and H. Chen, "Mapping the buried cable by ground penetrating radar and Gaussian-process regression," *IEEE Trans. Geosci. Remote Sens.*, vol. 60, 2022, Art. no. 4509912.

[7] S. Mohapatra and G. A. McMechan, "Prediction and subtraction of coherent noise using a data driven time shift: A case study using field 2D and 3D GPR data," *J. Appl. Geophys.*, vol. 111, pp. 312–319, Dec. 2014.

[8] C. Liu, C. Song, and Q. Lu, "Random noise de-noising and direct wave eliminating based on SVD method for ground penetrating radar signals," *J. Appl. Geophys.*, vol. 144, pp. 125–133, Sep. 2017.

[9] J. Xiao and L. Liu, "Suppression of clutters caused by periodic scatterers in GPR profiles with multibandpass filtering for NDT&E imaging enhancement," *IEEE J. Sel. Topics Appl. Earth Observ. Remote Sens.*, vol. 10, no. 10, pp. 4273–4279, Oct. 2017.

[10] D. Kumlu and I. Erer, "Clutter removal techniques in ground penetrating radar by using non-local means approach," *J. Fac. Eng. Architecture Gazi Univ.*, vol. 35, no. 3, pp. 1269–1284, 2020.

[11] X. K. He, H. Yan, C. Wang, R. Y. Zheng, Y. J. Li, and X. W. Li, "Non-stationary random noise removal in ground-penetrating radar images by using self-guided filtering," *Digit. Signal Process.*, vol. 129, Sep. 2022, Art. no. 103690.

[12] J. L. Starck, E. J. Candès, and D. L. Donoho, "The curvelet transform for image denoising," *IEEE Trans. Image Process.*, vol. 11, no. 6, pp. 670–684, Jun. 2002.

[13] R. Neelamani, A. I. Baumstein, D. G. Gillard, M. T. Hadidi, and W. L. Soroka, "Coherent and random noise attenuation using the curvelet transform," *Leading Edge*, vol. 27, no. 2, pp. 240–248, 2008.

[14] J. Baili, S. Lahouar, M. Hergli, I. L. Al-Qadi, and K. Besbes, "GPR signal de-noising by discrete wavelet transform," *NDT E Int.*, vol. 42, no. 8, pp. 696–703, Dec. 2009.

[15] B. Oskooi, M. Julayusefi, and A. Goudarzi, "GPR noise reduction based on wavelet thresholdings," *Arab. J. Geosci.*, vol. 8, pp. 2937–2951, 2015.

[16] L. Verdonck, F. Vermeulen, R. Docter, C. Meyer, and R. Kniess, "2D and 3D ground-penetrating radar surveys with a modular system: Data processing strategies and results from archaeological field tests," *Near Surf. Geophys.*, vol. 11, no. 2, pp. 239–252, Apr. 2013.

[17] X. N. Wang and S. X. Liu, "Noise suppressing and direct wave arrivals removal in GPR data based on Shearlet transform," *Signal Process.*, vol. 132, pp. 227–242, Mar. 2017.

[18] X. K. He, C. Wang, R. Y. Zheng, and X. W. Li, "GPR image noise removal using grey wolf optimisation in the NSST domain," *Remote Sens.-Basel*, vol. 13, no. 21, Nov. 2021, Art. no. 4416.

[19] G. Terrasse, J.-M. Nicolas, E. Trouvé, and É. Drouet, "Application of the curvelet transform for clutter and noise removal in GPR data," *IEEE J. Sel. Topics Appl. Earth Observ. Remote Sens.*, vol. 10, no. 10, pp. 4280–4294, Oct. 2017.

[20] Y. Yang and W. G. Zhao, "Curvelet transform-based identification of void diseases in ballastless track by ground-penetrating radar," *Struct. Control Health*, vol. 26, no. 4, Apr. 2019, Art. no. e2322.

[21] G. X. Chen, L. Y. Fu, K. F. Chen, C. D. Boateng, and S. C. Ge, "Adaptive ground clutter reduction in ground-penetrating radar data based on principal component analysis," *IEEE Trans. Geosci. Remote Sens.*, vol. 57, no. 6, pp. 3271–3282, Jun. 2019.

[22] Q. B. Su, B. Z. Bi, P. Y. Zhang, L. Shen, X. T. Huang, and Q. Xin, "GPR image clutter suppression using Gaussian curvature decomposition in the PCA domain," *Remote Sens.-Basel*, vol. 14, no. 19, Oct. 2022, Art. no. 4879.

[23] J. Li, C. Liu, Z. F. Zeng, and L. N. Chen, "GPR signal denoising and target extraction with the CEEMD method," *IEEE Trans. Geosci. Remote Sens.*, vol. 12, no. 8, pp. 1615–1619, Aug. 2015.

[24] T. Hao, L. Jing, and W. He, "An automated GPR signal denoising scheme based on mode decomposition and principal component analysis," *IEEE Trans. Geosci. Remote Sens.*, vol. 20, 2023, Art. no. 3500105.

[25] W. Xue, Y. Luo, Y. Yang, and Y. J. Huang, "Noise suppression for GPR data based on SVD of window-length-optimized Hankel matrix," *Sensors-Basel*, vol. 19, no. 17, Sep. 2019, Art. no. 3807.

[26] R. J. Oliveira, B. Caldeira, T. Teixidó, and J. F. Borges, "GPR clutter reflection noise-filtering through singular value decomposition in the bidimensional spectral domain," *Remote Sens.-Basel*, vol. 13, no. 10, May 2021, Art. no. 2005.

[27] L. Shao, R. Yan, X. Li, and Y. Liu, "From heuristic optimization to dictionary learning: A review and comprehensive comparison of image denoising algorithms," *IEEE Trans. Cybern.*, vol. 44, no. 7, pp. 1001–1013, Jul. 2014.

[28] Y. Gao, J. Y. Ma, and A. L. Yuille, "Semi-supervised sparse representation based classification for face recognition with insufficient labeled samples," *IEEE Trans. Image Process.*, vol. 26, no. 5, pp. 2545–2560, May 2017.

[29] Y. Chen et al., "Artifact suppressed dictionary learning for low-dose CT image processing," *IEEE Trans. Med. Imag.*, vol. 33, no. 12, pp. 2271–2292, Dec. 2014.

[30] D. L. Donoho, M. Elad, and V. N. Temlyakov, "Stable recovery of sparse overcomplete representations in the presence of noise," *IEEE Trans. Inform. Theory*, vol. 52, no. 1, pp. 6–18, Jan. 2006.

[31] D. L. Donoho and M. Elad, "On the stability of the basis pursuit in the presence of noise," *Signal Process.*, vol. 86, no. 3, pp. 511–532, Mar. 2006.

[32] M. Aharon, M. Elad, and A. Bruckstein, "K-SVD: An algorithm for designing overcomplete dictionaries for sparse representation," *IEEE Trans. Signal Process.*, vol. 54, no. 11, pp. 4311–4322, Nov. 2006.

[33] M. Elad and M. Aharon, "Image denoising via sparse and redundant representations over learned dictionaries," *IEEE Trans. Image Process.*, vol. 15, no. 12, pp. 3736–3745, Dec. 2006.

[34] X. Dong, J. Lin, S. Lu, H. Wang, and Y. Li, "Multiscale spatial attention network for seismic data denoising," *IEEE Trans. Geosci. Remote Sens.*, vol. 60, 2022, Art. no. 5915817.

[35] X. Dong, Y. Li, T. Zhong, N. Wu, and H. Wang, "Random and coherent noise suppression in DAS-VSP data by using a supervised deep learning method," *IEEE Trans. Geosci. Remote Sens.*, vol. 19, 2022, Art. no. 8001605.

[36] J. B. Luo et al., "GPR B-scan image denoising via multi-scale convolutional autoencoder with data augmentation," *Electronics*, vol. 10, no. 11, Jun. 2021, Art. no. 1269.

[37] Z.-K. Ni, C. Shi, J. Pan, Z. Zheng, S. Ye, and G. Fang, "Declutter-GAN: GPR B-scan data clutter removal using conditional generative adversarial nets," *IEEE Trans. Geosci. Remote Sens.*, vol. 19, 2022, Art. no. 4023105.

[38] H.-H. Sun, W. Cheng, and Z. Fan, "Learning to remove clutter in real-world GPR images using hybrid data," *IEEE Trans. Geosci. Remote Sens.*, vol. 60, 2022, Art. no. 5113714.

[39] A. Gaber, G. El-Qady, A. Khozym, T. Abdallatif, and S. A. M. Kamal, "Indirect preservation of Egyptian historical sites using 3D GPR survey," *Egypt J. Remote Sens.*, vol. 21, pp. S75–S84, Jul. 2018.

[40] M. Gaballah, M. Grasmueck, and M. Sato, "Characterizing subsurface archaeological structures with full resolution 3D GPR at the early dynastic foundations of Saqqara necropolis, Egypt," *Sens. Imag.*, vol. 19, Jul. 2018, Art. no. 23.

[41] A. Gaber, K. S. Gemail, A. Kamel, H. M. Atia, and A. Ibrahim, "Integration of 2D/3D ground penetrating radar and electrical resistivity tomography surveys as enhanced imaging of archaeological ruins: A case study in San El-Hager (Tanis) site, northeastern Nile Delta, Egypt," *Archaeological Prospection*, vol. 28, no. 2, pp. 251–267, Apr. 2021.

[42] Z. Liu, W. X. Wu, X. Y. Gu, S. W. Li, L. T. Wang, and T. J. Zhang, "Application of combining YOLO models and 3D GPR images in road detection and maintenance," *Remote Sens.-Basel*, vol. 13, no. 6, Mar. 2021, Art. no. 1081.

[43] H. Liu et al., "Detection of road cavities in urban cities by 3D ground-penetrating radar," *Geophysics*, vol. 86, no. 3, pp. Wa25–Wa33, May/Jun. 2021.
[44] J. G. Yang, K. G. Ruan, J. Gao, S. G. Yang, and L. C. Zhang, "Pavement distress detection using three-dimension ground penetrating radar and deep learning," *Appl. Sci.-Basel*, vol. 12, no. 11, Jun. 2022, Art. no. 5738.
[45] K. Dinh, N. Gucunski, K. Tran, A. Novo, and T. Nguyen, "Full-resolution 3D imaging for concrete structures with dual-polarization GPR," *Automat. Constr.*, vol. 125, May 2021, Art. no. 103652.
[46] K. Yan, Z. H. Zhang, and X. L. Xu, "Improved tucker decomposition algorithm for noise suppression of 3D GPR data in road detection," *Near Surf. Geophys.*, vol. 21, no. 2, pp. 138–151, Apr. 2023.
[47] S. Beckouche and J. W. Ma, "Simultaneous dictionary learning and denoising for seismic data," *Geophysics*, vol. 79, no. 3, pp. A27–A31, May/Jun. 2014.
[48] Z. J. Feng, "Seismic random noise attenuation using effective and efficient dictionary learning," *J. Appl. Geophys.*, vol. 186, Mar. 2021, Art. no. 104258.
[49] Y. K. Chen, "Fast dictionary learning for noise attenuation of multidimensional seismic data (expression of concern of vol. 209, pg. 21, 2017)," *Geophys. J. Int.*, vol. 221, no. 3, pp. 2053–2053, Jun. 2020.
[50] D. S. Feng, S. Liu, J. Yang, X. Y. Wang, and X. Wang, "The noise attenuation and stochastic clutter removal of ground penetrating radar based on the K-SVD dictionary learning," *IEEE Access*, vol. 9, pp. 74879–74890, 2021.
[51] S. K. Sahoo and A. Makur, "Dictionary training for sparse representation as generalization of -means clustering," *IEEE Signal Process. Lett.*, vol. 20, no. 6, pp. 587–590, Jun. 2013.
[52] S. K. Sahoo and A. Makur, "Image denoising via sparse representations over sequential generalization of K-means (SGK)," in *Proc. IEEE 9th Int. Conf. Inf., Commun. Signal Process.*, 2013, pp. 1–5.
[53] J. Wu, Q. L. Chen, Z. X. Gui, and M. Bai, "Fast dictionary learning for 3D simultaneous seismic data reconstruction and denoising," *J. Appl. Geophys.*, vol. 194, Nov. 2021, Art. no. 104446.
[54] R. Rubinstein, T. Peleg, and M. Elad, "Analysis K-SVD: A dictionary-learning algorithm for the analysis sparse model," *IEEE Trans. Signal Process.*, vol. 61, no. 3, pp. 661–677, Feb. 2013.
[55] D. L. Donoho, "Compressed sensing," *IEEE Trans. Inform Theory.*, vol. 52, no. 4, pp. 1289–1306, Apr. 2006.
[56] Y. C. Pati, R. Rezaiifar, and P. S. Krishnaprasad, "Orthogonal matching pursuit: Recursive function approximation with applications to wavelet decomposition," in *Proc. IEEE 27th Asilomar Conf. Signals, Syst. Comput.*, 1993, pp. 40–44.

Deshan Feng received the B.S., M.S., and Ph.D. degrees in geophysics from Central South University, Changsha, China, in 2000, 2003, and 2006, respectively.

From 2013 to 2014, he was a Senior Visiting Scholar with the Department of Earth Science, Rice University, Houston, USA. He is currently a Full Professor and the Director with the Department of Geophysics, School of Geosciences and Info-Physics, Central South University. He is a reviewer for IEEE TRANSACTIONS ON GEOSCIENCE AND REMOTE SENSING, *Computers and Geosciences*, and *Geophysics*. His research interests include the simulation wavelet analysis of electromagnetic waves.

Li He was born in Sichuan, China, in 2000. She received the B.S. degree in prospecting technology and engineering from Southwest Petroleum University, Chengdu, China, in 2022. She is currently working toward the M.S. degree in geological resources and geological engineering with the College of Geosciences and Info-Physics, Central South University, Changsha, China.

Her research interests include the data processing, target intelligent extraction, and recognition of ground penetrating radar.

Xun Wang was born in Henan, China, in 1990. He received the B.S., M.S., and Ph.D. degrees in geophysics from Central South University, Changsha, China, in 2013, 2016, and 2020, respectively.

He is an Associate Professor with the School of Geosciences and Info-Physics, Central South University. His research interests include the simulation of electromagnetic waves and the full-waveform inversion of ground-penetrating radar data.

Dr. Wang is a Reviewer for IEEE TRANSACTIONS ON GEOSCIENCE AND REMOTE SENSING, *IEEE Geoscience and Remote Sensing Letters*, *IEEE Access*, *Icarus*, *Applied Sciences*, and *Mathematical Problems in Engineering*.

Yougan Xiao photograph and biography not available at the time of publication.

Guoxing Huang photograph and biography not available at the time of publication.

Liqiong Cai photograph and biography not available at the time of publication.

Xiaoyong Tai photograph and biography not available at the time of publication.